Extreme events in the European renewable power system

van der Most, L.; van der Wiel, K.; Benders, R. M.J.; Gerbens-Leenes, P. W.; Kerkmans, P.; Bintanja, R.

Published in:
Renewable and Sustainable Energy Reviews

DOI:
10.1016/j.rser.2022.112987

Publication date:
2022

Renewable and Sustainable Energy Reviews 170 (2022) 112987

Contents lists available at ScienceDirect

Renewable and Sustainable Energy Reviews

journal homepage: www.elsevier.com/locate/rser

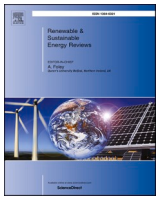

Extreme events in the European renewable power system: Validation of a modeling framework to estimate renewable electricity production and demand from meteorological data

L. van der Most [a,b,*], K. van der Wiel [b], R.M.J. Benders [a], P.W. Gerbens-Leenes [a], P. Kerkmans [c], R. Bintanja [a,b]

[a] Faculty of Science and Engineering, University of Groningen, Groningen, the Netherlands
[b] Royal Netherlands Meteorological Institute, De Bilt, the Netherlands
[c] Alpiq Trading, Prague, Czech Republic

ARTICLE INFO

Keywords:
Electricity model
Hydropower generation
Climate variability
Model validation
Extreme events
Extreme weather impacts
European energy transition
Compound events

ABSTRACT

With the need to reduce greenhouse gas emissions, the coming decades will see a transition of Europe's power system, currently mainly based on fossil fuels towards a higher share of renewable sources. Increasing effects of fluctuations in electricity production and demand as a result of meteorological variability might cause compound events with unforeseen impacts. We constructed and validated a modeling framework to examine such extreme impact events on the European power system. This framework includes six modules: i) a reservoir hydropower inflow and ii) dispatch module; iii) a run-of-river hydropower production module; iv) a wind energy production module; v) a photovoltaic solar energy production model; and vi) an electricity demand module. Based on ERA5 reanalysis input data and present-day capacity distributions, we computed electricity production and demand for a set of European countries in the period 2015–2021 and compared results to observed data. The model captures the variability and extremes of wind, photovoltaic and run-of-river production well, with correlations between modelled and observed data for most countries of more than 0.87, 0.68 and 0.65 respectively. The hydropower dispatch module also functions well, with correlations up to 0.82, but struggles to capture reservoir inflows and operating procedures of some countries. A case study into the meteorological drivers of extreme events in Sweden and Spain showed that the meteorological conditions during extreme events selected by the model and extracted from observational data are similar, giving confidence in the application of the modeling framework for (future changes in) extreme event analysis.

Lieke van der Most: Conceptualization, Methodology, Software, Validation, Formal analysis, Data curation, Writing - Original Draft, Visualisation. Karin van der Wiel: Supervision, Conceptualization, Writing - Review & Editing. Winnie Gerbens-Leenes: Supervision, Conceptualization, Writing - Review & Editing. René Benders: Supervision, Conceptualization, Writing - Review & Editing. Peter Kerkmans: Supervision, Richard Bintanja: Supervision, Conceptualization, Writing - Review & Editing.

1. Introduction

The transition towards low carbon electricity supply systems in the coming decades goes along with the replacement of fossil energy sources by renewable sources, mainly hydropower, wind and solar energy, and biomass. These renewable energy sources depend on the weather, e.g. the availability of sufficient water, wind, or solar radiation. Additionally, seasonal and interannual fluctuations in electricity demand are mostly determined by weather/climate [1]. These dependencies make renewable electricity supply vulnerable, variable, potentially non-dispatchable, and could affect the feasibility and reliability of future low carbon electricity supply systems. Recent events have shown how interannual variability in climate such as droughts [2,3], long-lasting high temperatures, and low wind speeds [4] can have devastating effects on the prices and security of critical energy services. With an increase in installed renewable capacities and electrification of other key sectors, this sensitivity to climate variability will only increase. Key aspects of successfully integrating more renewables are therefore: (i) the variability of the total renewable electricity generation on different time

* Corresponding author. Faculty of Science and Engineering, University of Groningen, Groningen, the Netherlands.
E-mail address: l.van.der.most@rug.nl (L. van der Most).

https://doi.org/10.1016/j.rser.2022.112987
Received 12 April 2022; Received in revised form 5 September 2022; Accepted 7 October 2022
Available online 17 October 2022

Abbreviations

CBS	Dutch Central Bureau for Statistics
ENTSO-E	European Network of Transmission System Operators for Electricity
JRC	Joint Research Centre
LSTR	logistic smooth transmission regression
MAD	median absolute deviation
ML	machine learning
PV	photovoltaic solar
RMSE	root mean square error
rRMSE	relative root mean square error
ERA5	the fifth generation atmospheric reanalysis of the global climate by the European Centre for Medium-Range Weather Forecasts
GMTED2010	Global Multi-resolution Terrain Elevation Data 2010

Symbols

C	merit
$\overline{cf}_{hydro}$	hydropower capacity factor
D_{net}	net demand after using all non-dispatchable sources *MWh*
E^{out}_{hydro}	energy dispatch hydropower reservoir *MWh*
E^{in}_{hydro}	theoretical energy inflow into reservoir *MWh*
E_{PV}	photovoltaic energy production *MWh*
E_{ror}	run-of-river hydropower production *MWh*
E_{wind}	wind energy production *MWh*
f_{ror}	fraction-of-discharge used by run-of-river hydropower
IC_{hydro}	the installed hydropower capacity *MW*
P^{in}_{hydro}	hydropower inflow potential *MW*
P_{ror}	run-of-river power output *MW*
Q_{ICh}	rated discharge of installed hydropower capacity $m^3\ s^{-1}$
$Q_{q=75}$	75th percentile discharge of an average year $m^3\ s^{-1}$
$T_{a,mean}$	population weighted daytime air temperature $^\circ C$
v_{ci}	cut in wind speed $m\ s^{-1}$
v_{co}	cut out wind speed $m\ s^{-1}$
v_r	rated wind speed $m\ s^{-1}$
α_1	model parameter - infliction point *MWh*
η_{res}	reservoir hydropower plant efficiency
η_{ror}	run-of-river hydropower plant efficiency
Δt	size of model time step hours *hours*
cf_{PV}	capacity factor photovoltaic solar
cf_{wind}	capacity factor wind
D	electricity demand *MWh*
f	fraction-of-discharge
F	logistic smoothing function
g	gravitational acceleration $m\ s^{-2}$
H	hydraulic head m
IC_{PV}	installed photovoltaic solar capacity *MW*
IC_{wind}	installed wind capacity *MW*
kx	recession coefficient
m	the number of years in the database years *years*
n	the number of timesteps in a year
Q	discharge $m^3\ s^{-1}$
ro_{accu}	accumulated runoff $m^3\ s^{-1}$
rdd	relative deviation difference variable
RES	country aggregated reservoir storage level *MWh*
rl	residual-load *MWh*
t	time days *days*
ρ	water density $kg\ m^3$

and spatial scales; and (ii) the possibility of accurately forecasting and strategically planning these fluctuations [5]. This makes the simulation of meteorological variability, extreme events, and climate change a key ingredient in strategic power system planning.

The extent to which renewable production technologies in Europe are sensitive to climate variability has been widely studied, but most of those studies focus on isolated production technologies [6,7] or demand [1,8]. Multiple studies have mentioned the importance of considering integrated energy systems [9–11], and have emphasized the relevance of analyzing those with extended periods of weather years to capture impact events based on climate variability [12].

A common current practice in energy modeling is the use of synthesized time series such as typical meteorological years or average availability factors in quantifying how impactful climate change is on the key metrics of the energy system. This could potentially lead to significant errors in studies examining a high renewable share. Due to the warming climate, the statistics and thus variability of weather changes. Additionally, there might be combined, non-linear, effects of variations in electricity production and demand as a result of relatively normal weather that could result in compound events with unforeseen extreme impact [13].

A number of previous studies analyzed variability [14,15] and extremes [16–18] in electricity demand and photovoltaic solar (PV) and wind generation under present and future climates. A key limitation of these studies is that they exclude hydropower production. Globally, hydropower is the most important renewable energy source. For example, in Europe there is an installed capacity of 123 GW producing 12% of Europe's electricity consumption [19]. Additionally, it plays an important role in the integrated impact of weather on the power system, as it can balance extremes in wind and PV production due to its dispatchable nature.

The main reason hydropower production is often excluded from such studies is that it is characterized by complex operating procedures [20]. Recent attempts to model the dispatch of country aggregated hydropower in Europe relied on the application of machine learning (ML) [21,22] or fitting parameters [23] to historic dispatch data from the European Network of Transmission System Operators for Electricity (ENTSO-E) Transparency Platform. Although these methods were reported to yield good results for run-of-river hydropower production [21,22], where the natural flow of river water flow is used to generate a base-load power, and decent results for reservoir hydropower operations, where dams with a large reservoir are used to store water [22], they come with a number of limitations. ML models can only be applied to predict the dispatch of the hydropower fleet from the training data, making it unsuitable for studying future energy systems. Additionally, due to a lack of historical ENTSO-E hydropower production data, the application of ML based techniques could potentially lead to overfitting. More importantly, extreme events cannot be diagnosed due to the use of short timeseries as training sets.

The application of ML models to historical data that are not representative of extreme scenarios or future climate can also be a problem in national electricity demand models. Demand models based on meteorological variables often apply ML techniques such as regression models to historic demand data [16,21]. Without regulating the behavior of the prediction of models for meteorological values outside of the training data, the predictive function might yield inaccurate results.

In this paper we present and validate a modeling framework that translates meteorological data into renewable electricity production and demand data aimed at scenario analyses of future renewable-dominated power systems under changing climate. We introduce four modules for the computation of production and demand: 1) a run-of-river hydropower production and 2) a reservoir hydropower inflow module based

on a routing scheme to approximate river discharge; 3) a hydropower dispatch module described as a linear programming problem that minimizes the difference between demand and renewable electricity productions over a timeseries where we push the solution to follow the national load curve; and 4) a demand module on a national level where we force a linear heating and cooling function to allow for extrapolation to temperatures that do not occur in the historic dataset.

In addition, we supplement these novel modules with PV and wind production modules from previous work [16], generate gridded installed capacity files from various databases, and validate all six modules on an aggregated country-level using ENTSO-E production and demand data and daily ERA5 reanalysis climate data [24]. Reanalysis combines models with past weather observations to produce (historic) gridded estimates of atmospheric, land, and oceanic climate variables. Furthermore, to assess how the modeling framework performs in selecting high-impact events, we apply it in a case-study of Sweden and Spain to analyze the meteorological conditions that lead to high impact events in the integrated power system and compare the results to ENTSO-E production data.

Although we validated the proposed framework for the current European power system with reanalysis data, it can easily be applied to simulate the meteorological risks and impacts on future power systems with a different/higher share of renewables and under different climate scenarios. The framework is suitable for analysis with large ensemble climate data on daily resolution. Two possible applications are 1) the selection of meteorological conditions of interest for the energy system, which can, in turn, be used on a higher resolution as input for higher resolution energy system models, or 2) the risk analysis of (long-lasting) extreme events in a highly renewable energy system that can be used to make large-scale tactical decisions for the energy transition such as additional (non-meteorological dependent) energy storage and non-renewable production requirements. Overall, this framework aims to be a step in bridging the disconnect between climate and energy modelers by providing a possible high-level step in an iterative trans-disciplinary process [12].

2. Description of modeling framework

Here we present the six modules that were used in the modeling framework. We calculated daily hydropower reservoir inflow and PV, wind, and run-of-river production for each grid cell. To validate the model, we aggregated the results to national levels. Demand and hydropower dispatch are also computed on a national level.

Fig. 1 shows a flowchart explaining how we converted meteorological data into electricity data, and which other (societal/energy system) data are used.

2.1. Demand module

Following the approach of [16] the relation between demand and temperature is described by applying a logistic smooth transmission regression (LSTR) model [25,26] to population weighted temperatures ($T_{a,mean}$) –temperatures in highly populated areas disproportionally impact energy demand– and historic demand (D).

The LSTR model allows for a smooth transition between the two linear regimes of heating demand due to low temperatures and cooling demand due to high temperatures:

$$D(t) = \left[\alpha_1 + \beta_1 T_{a,mean}(t)\right]\left[1 - F(t)\right] + \left[\alpha_2 + \beta_2 T_{a,mean}(t)\right]F(t)$$

With α_1, α_2 the zero intercepts and β_1, β_2 the slope of the linear heating and cooling regimes respectively. The logistic smoothing function F is expressed as:

$$F(t) = \left[1 + \exp\left(-\zeta\left(T_{a,mean}(t) - c\right)\right)\right]^{-1}, \zeta > 0,$$

With ζ a smoothing factor and c the infliction point. We account for different heating and cooling behavior between countries and days of the week by applying the LSTR model for each country individually and for weekends and weekdays separately. To allow for extrapolation of heating and cooling regimes towards extreme conditions, we force the linear regimes to cover at least 80% of the heating or cooling data though a number of steps. Each step is performed for weekend and weekdays demand data per country. The tipping point between heating and cooling regimes is determined by assessing the minimum point of the rolling average demand over a window of 10% of the countries' temperature range. Cooling and heating data are treated separately and the data is binned in 0.1 °C bins, resulting in a sequence of points. We then determine the linear regime of this sequence of points in accordance with the method presented by Ref. [27]. Next, we apply a linear regression fit to the demand data that fall within the temperature limits of the linear regime. The gradients resulting from this linear regression are forced in the cooling and heating regimes of the LSTR model (β_1 and

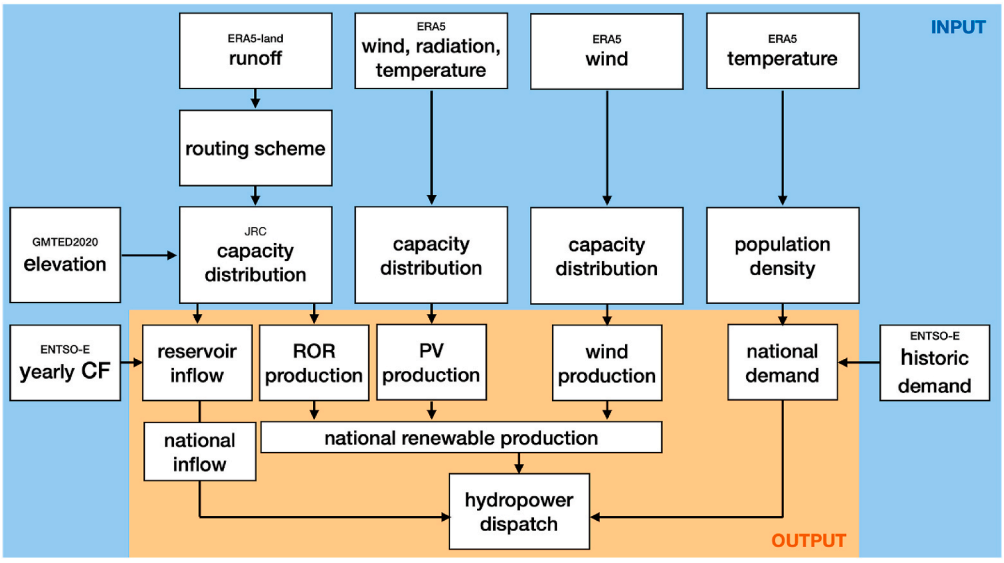

Fig. 1. Flowchart explaining how we converted meteorological data into electricity data. The flowchart gives a schematic overview of the modeling framework with in blue the inputs and in orange the outputs of the model. With the following abbreviations: ROR is run-of-river, CF is capacity factor, JRC is the Joint Research Centre, and PV is photovoltaic.

β_2). The above procedure was followed because applying an LSTR model to the demand and temperature data without this constraint can result in a fit in which the linear regimes lie mostly outside of the data (Fig. 2), making extrapolation to climate scenarios with more extreme temperatures unreliable. For each country, we assume that the maximum demand for cooling or heating is not higher than the maximum daily demand recorded in that regime during the weekend or weekday by ENTSO-E. Supplementary Information A provides tables with the fitting parameters and maximum heating and cooling demand for all European countries.

2.2. Photovoltaic solar energy production module

The daily PV energy production (E_{PV}) is computed according to:

$$E_{PV}(t) = IC_{PV} * \Delta t * \ cf_{PV}(t)$$

With IC_{PV} the installed PV capacity in the grid cell, Δt the timestep of the model and $\mathrm{cf_{pv}}$ the timestep capacity factor. Because the efficiency of a PV module is a result of its temperature, the timestep capacity factor depends on incoming solar radiation, windspeeds and daytime mean temperatures and is calculated assuming that all PV modules are placed horizontally and that they are operational during all daytime hours according to the method described in Refs. [16,29].

2.3. Wind energy production module

Similar to PV production, we computed wind energy production (E_{wind}) as:

$$E_{wind}(t) = IC_{wind} * \Delta t * cf_{wind}(t)$$

with, IC_{wind} the installed wind capacity in the grid cell and $cf_{wind}(t)$ the timestep capacity factor. The timestep capacity factor is computed with a cubic power curve, with onshore and offshore specific cut-in, rated and cut-out windspeeds (v_{ci}, v_r and v_{co} respectively). Meteorological wind data is typically available at a standardized height of 10 m. For the computation of the capacity factor the 10 m wind speed is scaled to hub height with the power law [30]. We neglected downtime of the wind turbines for maintenance. For a full description of the method see Ref. [16].

2.4. Hydropower reservoir energy inflow module

For the approximation of hydropower reservoir water inflow, we route runoff data along flow direction routes to form discharge patterns. To reduce the computational time, this routing is done at $0.5^\circ \times 0.5^\circ$ resolution. The routing scheme starts at the grid cells with no accumulation (the highest point in the basin) and follows the flow direction downstream, adding the accumulated runoff to the locally generated runoff. We approximate discharge delays with a flow recession coefficient such that [31]:

$$Q(t) = (1 - kx) * ro_{accu}(t) + kx * Q(t-1)$$

With Q the cell discharge, kx the recession coefficient and ro_{accu} the accumulated runoff. Delays due to water accumulation in lakes or reservoirs, anthropogenic water usages and water management, such as dams, are not considered. With the resulting discharge, we calculate the available hydropower (P_{hydro} $[MW]$) per grid cell as:

$$P^{in}_{hydro}(t) = \rho\ g\ H\ \eta_{res}\ (Q(t) * f)\ , f \leq 1$$

With ρ the water density ($998\ kg\ m^3$), g the gravitational acceleration ($9.81\ m\ s^{-2}$), H the hydraulic head and η the constant hydropower plant efficiency. In reality, hydropower turbine efficiencies will depend on the discharge and available head.

To allow for the use of large grid cells we assign a fraction-of-discharge ($f[\ -\ ]$) to each grid cell based on the installed hydropower capacity (see Fig. 3). We determine this factor by using the yearly mean capacity factor and a mean yearly cumulative discharge in the grid cell according to:

$$f = \frac{\sum_{y=0}^{m} \frac{\sum_{t=0}^{n} Q(t)}{m}}{Q_{ICh} * \Delta t * n * \overline{cf}_{hydro}}$$

With m the number of years in the dataset, n the number of timesteps per year, Δt the number of hours per timestep, Q_{ICh} the rated discharge of the installed capacity and $\overline{cf}_{hydro}$ the mean annual hydropower capacity factor in the grid cell expressed as the ratio of power generated to the hypothetical maximum of the installed capacity for a specific time period. The rated discharge is expressed as:

$$Q_{ICh} = \frac{IC_{hydro}}{\rho\ g\ H\ \eta}$$

With IC_{hydro} the installed hydropower capacity in the grid cell. We assume that all incoming discharge into the reservoir in an average year is used by the powerplant during that year. Because f gives the ratio of incoming water and potential energy production in a grid cell, it corrects for anthropogenic water consumption and reservoir evaporation. We express the available reservoir hydropower energy, ($E^{in}_{hydro}(t)$), as the sum of the daily available hydropower and the timestep in hours:

$$E^{in}_{hydro}(t) = P^{in}_{hydro}(t) * \Delta t$$

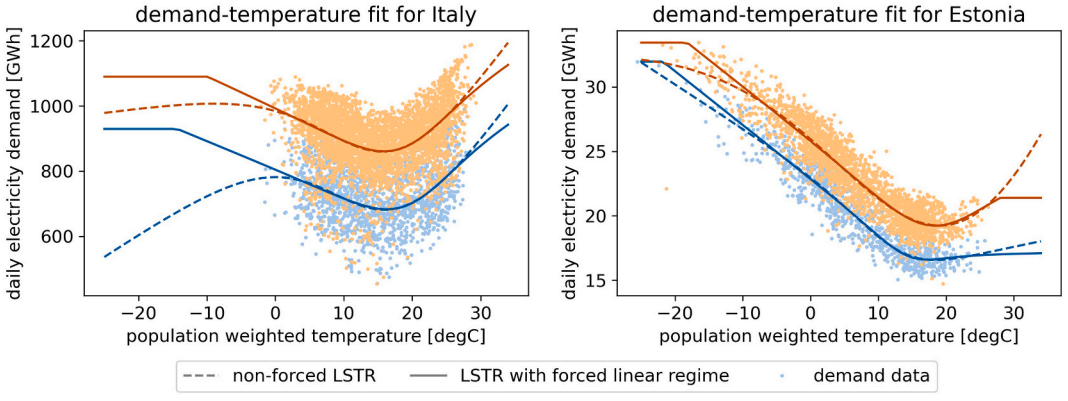

Fig. 2. LSTR model fit for Italy and Estonia with (solid line) and without (dashed line) linear regime forcing. In orange the weekday and in blue the weekend demand data [28].

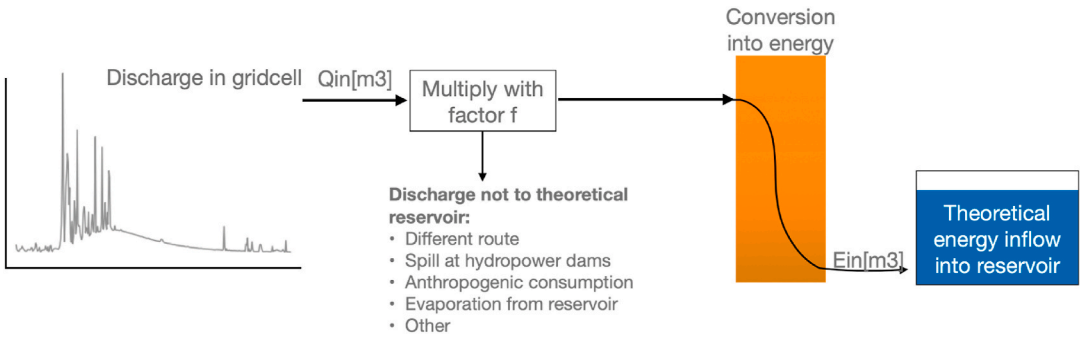

Fig. 3. Schematic of the hydropower reservoir inflow module and the application of the fraction-of-discharge.

2.5. Hydropower run-of-river production module

The utilizable discharge water volume of run-of-river hydropower plants depends on the installed capacity in the grid cell. Runoff hydropower plants are often designed with an exceedance between 10 and 40% [32]. Above the installed capacity (a cut-off or threshold level), the plant cannot harness discharge. We assume the average probability and selected an exceedance of 25%, reflecting the probability that the discharge will exceed the rated discharge. Similar to the hydropower reservoir inflows, the factor f_{ror} corrects for the discharge fraction in the grid cell used by the hydropower plants, defined as the ratio between the maximum discharge of the installed capacity and the 75th percentile discharge of an average year ($f_{ror} = Q_{q=75}/Q_{IC}$). We assume that run-of-river plants have no reservoir storage capacity. The run-of-river power output, (P_{ror}), is expressed as:

$$P_{ror}(t) = \rho\, g\, H\, \eta_{ror}\, (Q(t) * f_{ror}), \quad f_{ror} \leq 1\,,$$

Since we assume no downtime due to maintenance, the available run-of-river electricity production (E_{ror}) is a function of the available power and the timestep of the model:

$$E_{ror}(t) = P_{ror}(t) * \Delta t$$

2.6. Aggregated hydropower reservoir dispatch module

In contrary to wind, PV solar and run-of-river hydropower production, hydropower reservoir production is a dispatchable source of energy. As long as there is water available in a reservoir, its power output can be adjusted according to demand at the request of power grid operators. To approximate this decision-making process, we formulate the national dispatch of hydropower energy as a moving horizon linear programming problem that minimizes the total difference between electricity demand and renewable electricity productions (residual-load) over a timeseries, while we push the solution to follow the national load curve so as to minimize the maximum residual-load ($rl_{max}\,(t)$). We move the horizon with steps of 28 days and run the minimization problem for windows of a year. We assume that all non-dispatchable renewable sources are fully used before using reservoir hydropower (E^{out}_{hydro}) such that:

$$rl(t) + E^{out}_{hydro}(t) \geq D_{net}(t)$$

Where D_{net} is the net demand after using all non-dispatchable sources ($D_{net} = D - E_{ror} - E_{wind} - E_{PV},\ D_{net} \geq 0$) and *rl* is the residual-load. We set the aggregated country reservoir storage level (*RES*) to be the same at the beginning and the end of the timeseries and express it as a basic water balance that neglects any form of evaporation or condensation:

$$RES(t) = RES(t-1) + E^{in}_{hydro}(t-1) - E^{out}_{hydro}\,(t-1)$$

We set the reservoir storage level at the beginning of each optimization window to match the storage level at the end of the 28th day of the previous window, and the storage level at the 14th day of the optimization window to the reservoir level on the 42nd day of the previous window. This forces a 14-day overlap between the two optimization windows; which prevents sudden jumps in the dispatch and maintains the water balance between windows.

To approach a realistic dispatch and prevent an overoptimized output, but fill reservoirs with foresight for the rest of the year, we construct the optimization input from two different sources. The first 42 days of the inflow and net demand input values come from the daily variables computed with the production and demand modules described above (prediction). On the other days of the optimization window, they are based on a mean estimation. Additionally, to prevent the optimization from draining the reservoir, we use mean estimated reservoir levels to set a minimum reservoir level at the end of the moving window. Fig. 4 shows a schematic example of the hydropower reservoir dispatch results from three moving optimization windows and how they contribute to the output.

The reservoir sizes are bound by a maximum storage capacity and the daily energy production is constrained by the installed hydropower plant capacity. Additionally, to push the solution to follow electricity demand we define a relative deviation difference variable (*rdd*). Under the assumption that $\sum E^{out}_{hydro}(t) = \sum E^{in}_{hydro}(t)$ we express *rdd* as:

$$rdd(t) = \frac{\mathrm{D_{net}(t)} - \overline{\mathrm{D}}_{net}}{\overline{\mathrm{D}}_{net}} - \frac{E^{out}_{hydro}(t) - \overline{E}^{in}_{hydro}}{\overline{E}^{in}_{hydro}}$$

We define the objective function to minimize the total and maximum residual load and push dispatch to follow demand as:

$$\min\left(\sum\left[C_{rl} * \ rl(t) + C_{hydro} * \ E^{out}_{hydro}(t) + rdd(t)\right] + rl_{max}\right)$$

With C_{rl} and C_{hydro} expressing the merit order of residual-load and hydropower respectively. It should be noted that since *rdd* is a relative value it is several orders of magnitude smaller than the demand and hydropower production. Its influence on the total cost of the system is small, but when there are multiple solutions that result in (approximately) the same residual-load, the solution that follows the net demand best is favored. Fig. 5 shows the effect of adding the *rdd* and $\mathrm{rl_{max}}$ to the objective function. The difference between the total residual-load over the timeseries of 7 years for the different objective functions for Sweden is only 2.3%.

3. Methodology and data

The overall validation methodology includes the preparation of meteorological data, computation of country-specific demand fits, generation of installed capacity maps, selection of validation data and analysis of the modeling framework performance.

We ran the modules for present-day installed capacities of renewable energy technologies and with historic meteorological data on a daily timestep ($\Delta t = 24\,h$) for the European countries. We compared the modelled results to electricity production and demand data from

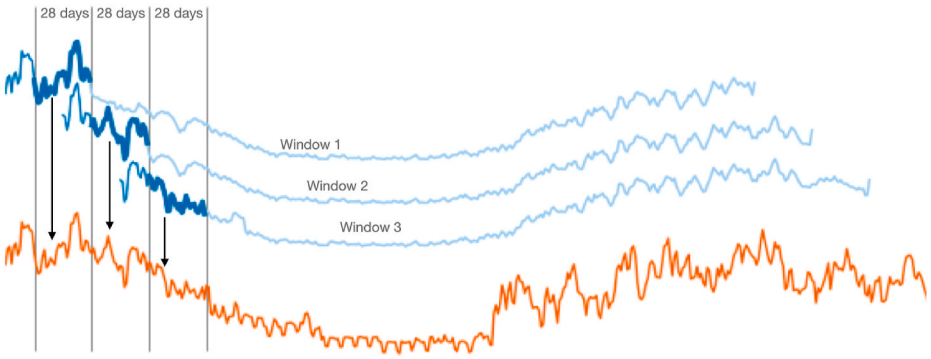

Fig. 4. Illustrative overview of three moving horizon optimization windows (in blue) and how they contribute to the output (in orange). With the results on the timesteps with prediction input values (thick lines) and the results on the timesteps with mean estimated values (thin lines).

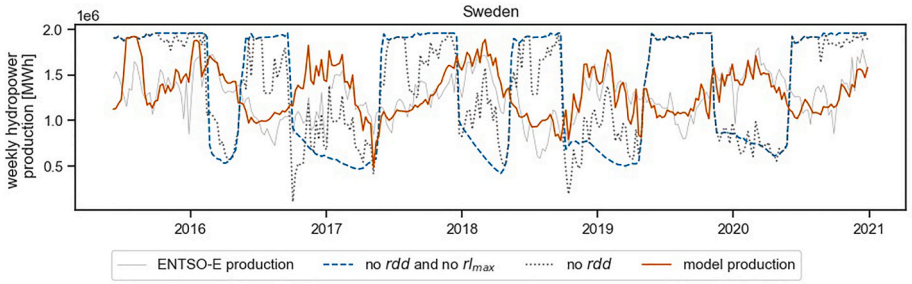

Fig. 5. *Results of hydropower reservoir dispatch optimization for objective function with (orange line) and without relative deviation difference between demand and dispatch (rdd) (grey dashed line) and maximum residual load (rl_{max}) (blue dashed line) in the minimization objective function. With the ENTSO-E production* [28] *as a reference (grey line).*

ENTSO-E [28]. Fig. 6 shows the European countries that are included in the validation.

3.1. Meteorological input data

For the computation of demand and renewable energy production we used a total of five meteorological variables. Three meteorological variables were collected from the ERA5 reanalysis dataset [24] as input for the wind and PV solar production and demand modules: 10 m wind speed [m s^{-1}], near-surface temperature [°C] and solar irradiance [kW m^2]. The ERA5 data are available on a 30 km^2 grid and at hourly timesteps, and we resampled them to daily timesteps. Runoff [m/timestep] was collected from the ERA5-land database [33], remapped to a 0.5° × 0.5° resolution and summed to daily timesteps for the computation of hydropower production. Since the ENTSO-E transparency platform has data starting from 2015, the reanalysis data were collected for the period 2015–2021.

Fig. 6. In orange the countries that are included in the validation.

3.2. Installed capacities

The geospatial information of the renewable powerplants installed capacities were collected from various sources and combined into grids with the resolution of the meteorological variables. For the validation we took the year 2020 as a reference (Fig. 7).

The locations and power capacity estimations of PV and wind farms (groups of modules or turbines in the same location) were computed based on OpenStreetMap data of 2020 according to the method presented by Ref. [34]. We converted the coordinate data to gridded data by summing the installed capacities of all the farms that fall into a grid cell. Due to the differences in height, capacities, and power curves of offshore and onshore wind turbines, we modelled the two types separately. Because the computation of energy farms with Dunnets method [34] resulted in almost no offshore locations, additional open source data were used to generate gridded data of installed offshore wind capacities [35]. EMODnet provides vector data in the form of polygons on offshore windfarms and their capacities in European seas. We converted the available shapefiles to gridded data by evenly distributing the installed capacity of the offshore windfarm over all the grid cells that overlap with the windfarm polygons in the dataset.

We extracted run-off-river and reservoir hydropower plant locations from the Joint Research Centre (JRC) Hydro-power database [36]. That dataset contains geospatial and capacity information of many European hydropower plants, but lacks hydraulic head data for 60% of the plants. Therefore, we approximated the hydraulic head by taking the difference between the maximum and minimum elevation based on GMTED2010

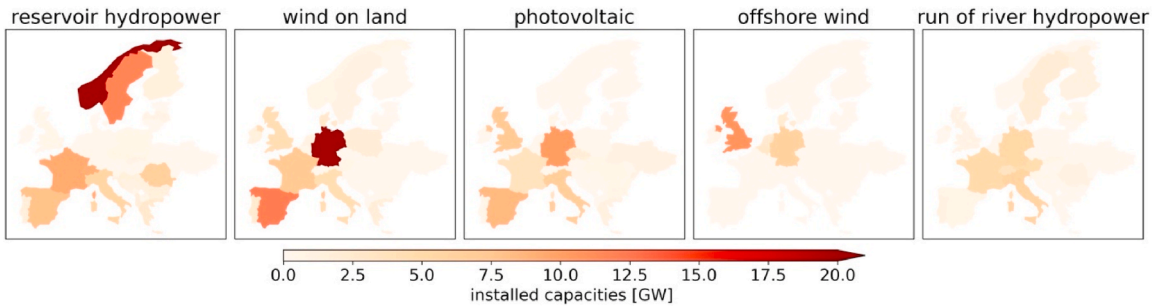

Fig. 7. Aggregated installed capacities for renewable power plants in Europe 2020 as used in the validation.

elevation data of 25 m resolution [37]. For reservoir plants, the difference between maximum and minimum elevation was linearly fitted to the available hydraulic head data in the JRC database. Because of the use of penstocks and cascade reservoirs, the hydraulic head of reservoir hydropower plants can be the result of an altitude difference that covers more than the grid cell size of 25 m. This was accounted for by computing the altitude difference from a grid box covering multiple grid cells. To determine the size of the grid box that yields results that best approximates the hydraulic head, we compared the correlation relation between elevation difference and reservoir hydropower plants hydraulic head of the JRC database for different grid box sizes. The highest correlation (0.62) occurred for a box of 11 × 11 grid cells around the coordinates of the reservoir hydro plant (see Fig. 8).

For run-of-river powerplants, we estimated the hydraulic head as the altitude difference within the grid cell. We assigned a hydraulic head of 1.8 m to all powerplants in grid cells without elevation difference, corresponding to the minimum hydraulic head in the JRC database. We assigned these estimated heights to each hydropower plant in the dataset, and combined the dataset into a 0.5° × 0.5° grid by taking the sum of the installed capacity and the capacity weighted hydraulic head for all powerplants in a grid cell.

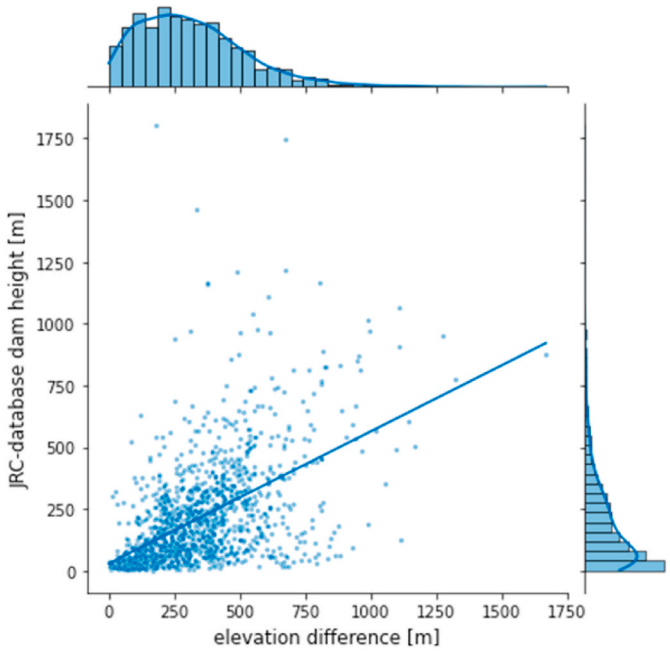

Fig. 8. Linear relation between elevation difference in 11 × 11 gridbox of GMTED2010 data [37] and reservoir hydropower plants hydraulic head of JRC database [36].

3.3. Demand module input data

We applied the LSTR model for each country to historic demand data from the ENTSO-E data portal and transparency platform [28] and to population weighted temperatures computed from 1 km Worldpop data [38] and ERA5 near surface temperature data [33], aggerated on national level. We remapped the population data to the ERA5 grid by summing all values within larger grid cells.

We applied the LSTR model to demand data for the period 2006–2021 for all European countries, except for Albania and Belarus (due to a lack of data). Prior to applying the regression model, we cleaned the ENTSO-E demand data in three steps. First, by means of a visual inspection of the country demand data over time, we removed years with unreliable looking data from the dataset. For example sudden demand increases or decreases, periods with missing data, and very irregular data.

Secondly, to remove outliers from the data we applied a median absolute deviation (MAD) filter [39]. Since the demand data are subject to seasonal changes, we used the MAD filter on monthly bins to select monthly outliers, assuming a normal distribution (consistency constant of 1.4826) and a conservative threshold of 3.5 [39]. Less conservative thresholds resulted in the removal of low or high demand values that could be explained by the seasonal nature of demand.

Thirdly, since we are looking for the relation between temperature and demand, we removed days of the year that repeatedly showed a statistically lower electricity demand (often due to social behavior) than expected at a given daily temperature from the dataset. For each country, we grouped the daily demand values in one-degree temperature bins, and the days of the year that occurred more than 70% of the time in the lowest 25% of a bin were removed. For all countries, we removed 50 different days of the year. For all countries, except Moldova, Montenegro and Bulgaria, the statistically removed days were public holidays. Fig. 9 shows the distribution of removed days of year per country. Countries that are not in the figure did not have any days removed. The days that were most often removed were 26th of December (in 24 countries) and the 1st of May (in 20 countries). See Supplementary Information A for detailed information and figures of the ENTSO-E data used for the LSTR model.

3.4. Validation input parameters

Supplementary Information B gives an overview of the input parameters used for the validation. The power curves for offshore and onshore wind turbines were determined by running the modules for different settings and selecting values that resulted in the highest correlation between modelled production and ENTSO-E wind energy production. The delay in discharge is approximated by applying the same recession coefficient to all grid cells. Similar to the power curves, this coefficient was selected by analyzing the correlation between the run-of-river hydropower module and ENTSO-E production for different values. Also, the hydropower storage capacities were determined based on different optimization runs and comparing correlations between the

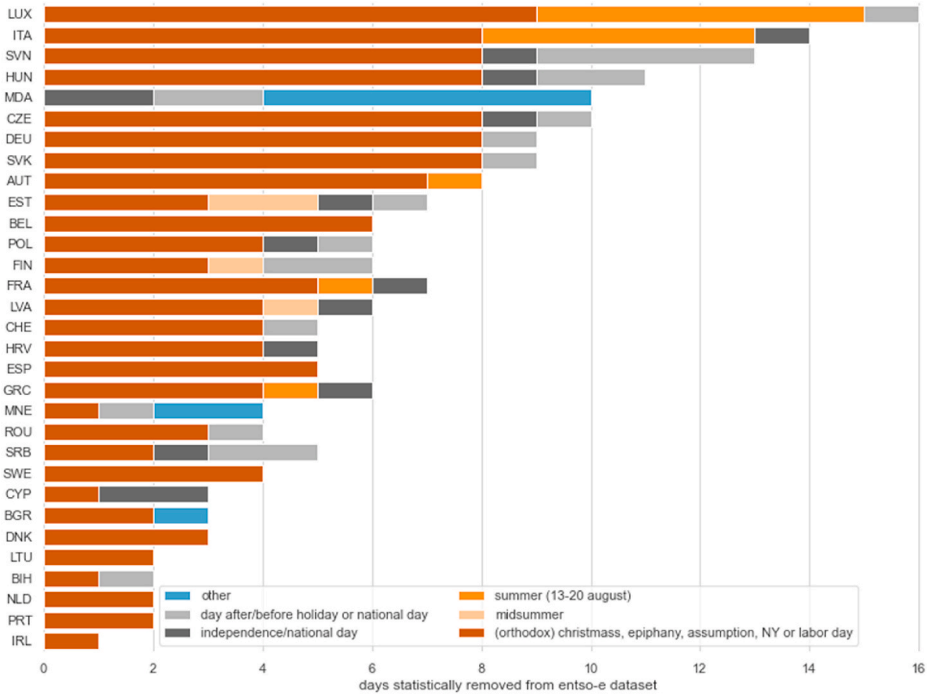

Fig. 9. Number of days with statistically low energy use in temperature bins of one-degree Celsius for European countries that were removed from the ENTSO-E load data before applying the LSTR model. Countries that are not in the figure did not have days removed. Abbreviation of country names can be found in Supplementary Information C.

runs and observed data.

3.5. Validation data

To validate the computed renewable energy production and demand, we compared the country aggregated outcomes to data from the ENTSO-E transparency database. We collected five production types for validation: (i) offshore wind; (ii) onshore wind; (iii) solar PV; (iv) hydropower reservoir; and (v) hydropower run-of-river. Production was resampled to daily data. Since we are interested in validating interannual variability, we deleted all countries that have less than one year of data from the ENTSO-E dataset.

Additionally, weekly stored energy values for hydro reservoir and storage plants were retrieved to approximate hydropower reservoir inflow values. We deducted the historical weekly hydropower inflow data (E^{in}_{hydro}) from the weekly aggregated production ($E_{hydro,val}$) and the difference in reservoir filling ($RES_w[MWh]$) between the beginning and end of the week:

$$E^{in}_{hydro,val}(w) = RES_{val}(w+1) - RES_{val}(w) - E_{hydro,val}(w)$$

There are a number of countries with installed renewable capacities in the model but no generation data in ENTSO-E, or vice versa. We removed these energy technologies from the validation and excluded them in the total renewable energy production metric. Table 1 gives an overview of the removed countries. Additionally, the installed capacity in the model and the reported yearly installed capacities by ENTSO-E are not the same. To allow for a comparison between the observed and modelled data we normalize the production values over the installed capacities to get the capacity factor timeseries. The ENTSO-E installed capacities are available as yearly data-points, which we linearly interpolated to correct for the trend in installed capacities. For reservoir and run-of-river hydropower production we deleted some sections of unreliable looking ENTSO-E data prior to validation, see Supplementary Information D for details.

Table 1
Countries that we removed from the model and ENTSO-E data for the validation of the model. Abbreviation of country names can be found in Supplementary Information C.

	Countries removed from model	Countries removed from ENTSO-E
Onshore wind	UKR, LUX, SVK	MKD, SVN
Offshore wind	ESP, SWE	
PV	UKR, CYP, EST, FIN, IRL, LUX, LVA, NOR, POL, SRB, SWE	
Run-of-river	BIH, GRC, MNE, SWE	NOR, EST, LTU
Hydro reservoir	BEL, FIN, IRL, LVA, MKD, SVN, GBR	

3.6. Evaluation of the modeling framework

To evaluate the accuracy and performance of the electricity and demand modules, we used the following metrics: the root mean square error (RMSE), the relative root mean square error (rRMSE), the coefficient of correlation (r) and the z-score.

Pearson's coefficient of correlations provides information on the strength of the linear relationship between the ENTSO-E and modelled values. The RMSE describes the average difference between the modelled data and the electricity observations by ENTSO-E in units of the observed value. To provide a relative measure (rRMSE), we normalized the RMSE to the mean daily validation data. The z-score provides a measure of how far a data point is from the mean, expressed in terms of standard deviations. If the z-score is zero, the outcome equals the mean. We used the z-score to find the most extreme anomalies in the modelled data and validation data. To correct for seasonality, the z-score is defined to data grouped per week of the year. The largest and smallest z-score of the time-series describes the largest anomalies in the dataset.

By using the capacity factors for the model validation, the accuracy of the ENTSO-E values becomes highly dependent on the correspondence between their reported installed capacities (once a year) and their

timeseries production data. We found multiple sections of the ENTSO-E data where this led to unrealistic capacity factors (very low, higher than 1, or sudden yearly jumps), suggesting that the reported installed capacity is not reliable. Therefore, we mainly report on correlation between values; any absolute measures such as RMSE should be interpreted with care.

4. Results and discussion

In presenting the analysis on overall performance of the modeling framework, we will show results for all countries but highlight two: Sweden and Spain. We focus on these two countries because both Spain and Sweden have all four renewable production technologies installed in the model, but have different demand profiles (summer cooling through air-conditioning in Spain, but not in Sweden) and hydropower operations (seasonal in Sweden and more short-term in Spain), resulting in different system responses to meteorological drivers. The results of all other countries can be found in Supplementary Information E.

4.1. Overall model performance

4.1.1. Demand

Fig. 10 shows the ENTSO-E and modelled demand time series for Sweden and Spain in 2021. To allow for evaluation of the demand module, we trained the demand module with temperature data up to July 2021 and used the second half year of 2021 as testing data. Sweden has high heating demands in colder seasons and a long period of lower demand in summer, suggesting little to no use of air-conditioning. In Spain, there is an elevated electricity demand both in summer and in winter, corresponding with a heating and cooling demand. Both for Sweden and Spain, the seasonal cycles determined by their respective climates are captured well by the demand module.

Furthermore, in both countries we observe a weekly cycle that is most likely the result of human activity and social behaviors [1]. In the module we approximate this with separate weekend and weekday LSTR which works well on most days of the week, but results in an overestimation of the demand on Sundays in Spain (Fig. 10).

4.1.2. Production

With mean values across all countries larger than 0.86, correlations are high for wind, offshore wind and PV solar production. However, we find substantial regional differences in model performance for run-of-river and reservoir hydropower (Fig. 11).

4.1.3. Wind energy production

Both onshore and offshore wind production have a mean correlation of 0.87 and a coefficient of determination exceeding 0.75, showing that there is a strong linear association between the modelled and validation data that explains a large part of the variation in data. Consequently, countries that have a large share of wind and PV solar in their renewable mix, e.g. Denmark and Germany, have a high model performance for their total renewable electricity production (Fig. 11). However, the module structurally overestimated wind electricity production in the higher ranges of capacity factors, resulting in a high rRMSE ranging from 37% to 50% for offshore winds and from 27% to 358% for onshore winds (Fig. 12). This can have a number of causes: the actual average rated windspeed of the turbines is higher than the values used in the module, the computed wind speeds at hub-heights of the wind turbines are too high, the operational time of 24 h per day is a significant overestimation or there is a bias in the ERA5 data. The high rRMSE in combination with a high correlation can sometimes be explained by the aforementioned discrepancy between installed capacity and reported electricity production in the ENTSO-E data. An example is the Netherlands ($r = 0.94$ and rRMSE = 358% for onshore wind); i.e. the installed capacity reported by ENTSO-E is similar to the installed capacity reported by the Dutch Central Bureau for Statistics (CBS) [40], but the computed capacity factor from the ENTSO-E data (0.11 in 2019) is more than 2 times smaller than the one reported by CBS (0.26 in 2019): not all wind energy production is reported by ENTSO-E, explaining the high rRMSE.

4.1.4. PV solar energy production

The PV module follows the daily, seasonal and inter-annual variability of solar PV production well for most countries, but slightly overestimates production in summer (Figs. 11 and 12). For countries with relatively lower correlations such as Great Britain and the Netherlands ($r = 0.68$ and $r = 0.74$ respectively), the ENTSO-E capacity factor data show year-to-year jumps as a result of increases in reported installed capacities that don't correspond with increases in production (see Supplementary Figure E−2). Isolating the year 2020 results in correlations >0.97, again implying an error in the reported yearly

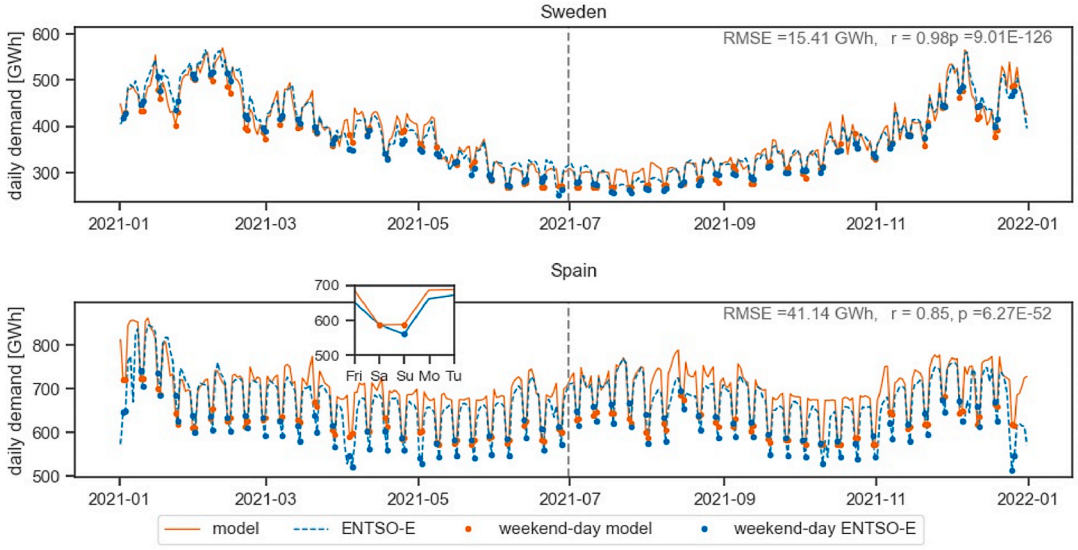

Fig. 10. ENTSO-E (blue dashed line) and modelled (orange line) demand timeseries [28] of Sweden and Spain with the dashed grey line marking the transition between training data of the demand module (left of line) and testing data (right of line). The dots on the graph mark weekend-days. With r the correlation coefficient, p the statistical significance and RMSE the Root Mean Squared Error between ENTSO-E and modelled demand of the testing dataset (from July 2021). The insert in Spain shows a zoom-in of the demand during the third week of April.

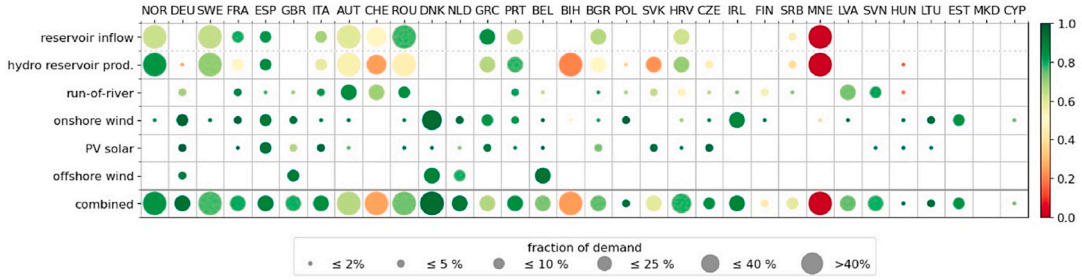

Fig. 11. Correlation between modelled and ENTSO-E data [28], presented per technology type. Green circles indicate a correlation close to 1, red circles indicate *r* is close to 0. Blank spaces indicate that there is no ENTSO-E and/or modelled data for these technologies in associated countries. For countries that show a correlation for reservoir hydropower production but not for reservoir inflow, ENTSO-E does not have reservoir storage values. The size of the circle gives an indication of the contribution of that technology to national electricity demand. For onshore/offshore wind and solar *r* is based on daily values, for run-of-river/reservoir hydropower and the combined technologies the *r* values are based on weekly means. The correlation of reservoir inflow is added as a reference for hydropower reservoir production.

change of installed capacities. This has previously been noted by Ref. [41].

4.1.5. *Run-of-river hydropower production*

For most countries, seasonal and interannual variability is captured well by the run-of-river hydropower's module. Only three countries have weekly correlations below 0.65: Hungary, Croatia and Finland (Fig. 11). The reason for the low performance in those countries is unclear and could be found in either the location of installed capacities, accuracy of climate input data and routing scheme, quality of observed data, and/or the module assumptions. Fig. 12 reveals that the module performs poorly on daily variability for all countries. One explanation for this could be that we assumed that run-of-river hydropower plants have no storage available, but in reality, many run-of-river plants will have a small water storage behind a weir storing enough water to allow for load balancing for a week or even more. Additionally, the delay approximation using recession coefficients apparently is not accurate enough to model daily discharge variability.

4.1.6. *Reservoir hydropower dispatch*

The reservoir dispatch module captures hydropower production, characterized by complex operating procedures, surprisingly well for many countries (Figs. 11 and 12). The correlations we found are only slightly lower than those in a recent study that applied a random forest model to the ENTSO-E data to reconstruct run-of-river and reservoir hydropower generation [22], and it outperforms the dispatch optimization model applied by Ref. [23] in capturing historical seasonal dispatch for Norway and Spain. Montenegro, Bosnia and Herzegovina and Switzerland have a large share of hydropower that is poorly captured by the module, however. These countries already show a low correlation between the modelled inflow and ENTSO-E data. As with the countries with poorly modelled run-of-river productions, it is difficult to determine the exact cause. One possible explanation could be that the inflow into the hydropower reservoir is not related to the natural discharge of the river due to, for example, cascading reservoirs. Fig. 13 shows that the module is able to estimate hydropower production in decent correlation with observed data for both countries with long-term and shorter-term storage. High incoming discharges in Sweden occur in summer as a result of snowmelt. The incoming discharge is stored until winter when Sweden experiences a peak in demand and it is dispatched. The module reproduces this behavior well. Even though the module underestimates the delay in incoming discharge in Sweden, showing a peak later in summer compared to the ENTSO-E data, this is made up for by the dispatch optimization. In general, delayed or earlier peaks in inflow as a result of the simplified routing scheme can at least partially be "corrected" by the dispatch module.

In Spain there is a high correlation between inflow and dispatch, suggesting that, in general, there is no long-term storage in Spanish reservoirs. The module captures the seasonal and interannual variability well (see lower production in spring 2017 and 2019 in Spain), but has difficulty capturing week-to-week variations as a result of control decisions.

4.2. *Prediction of extreme events*

To analyze the modeling framework's performance in selecting days with statistically low energy production, we computed the z-score for 7-days rolling mean capacity factors, relative to the timeseries' mean capacity factor and standard deviation of that weekly period. Fig. 14 shows the fraction of events that overlap between the modelled and ENTSO-E lowest 10% z-score. Statistical extremes in ENTSO-E PV capacity factors are not always captured well by the model. This can mostly be explained by the variations in ENTSO-E data. Countries with a poor capture of extremes correspond with countries that have jumps in reported yearly-installed capacities, resulting in large year-to-year variations in capacity factors (see Supplementary Figure E−2). The model selects statistical extremes in onshore and offshore wind well, whereas the run-of-river and reservoir hydropower events do not correspond well. This is expected, as the exact date of the events are compared, and both the hydropower and run-of-river production are subject to shifts in timeseries between modelled and ENTSO-E data as explained above.

4.2.1. *Case study validation: meteorological conditions during low production and high demand in Sweden and Spain*

To get more insight in what drives (the difference between) modelled and ENTSO-E events, we present a case study into the meteorological conditions during high residual-loads. Fig. 15 compares the top-7 modelled events with highest national 7-day residual-load against the ENTSO-E events. The events are selected so they have no overlap and be a minimum of 7 days apart. Small shifts in time of events can be explained by time lags in hydropower production. Although events do not take place at exactly the same day, they can be the result of similar meteorological drivers.

For Sweden, all events take place in winter, corresponding with their high demand (Fig. 10) and low hydropower inflow (Fig. 13) in winter. Both in the model and the ENTSO-E composites we observe a ridge of high pressure from West to central Europe during events, bringing relatively cold northerly winds to Northern-Europe (Fig. 16). However, the ridge is located a bit more north and extends to Eastern-Europe in the model-based composites. The high residual-load in Sweden is mostly driven by high demand as a result of low temperature anomalies.

For Spain, Fig. 15 shows that three of the high-residual events in the ENTSO-E data take place in summer, when high temperatures increase the cooling demand. The model does not capture these summer events well: the top 20 events predicted by the model contains only 3 summer events. For fair comparison of events in the composite, we limit ENTSO-

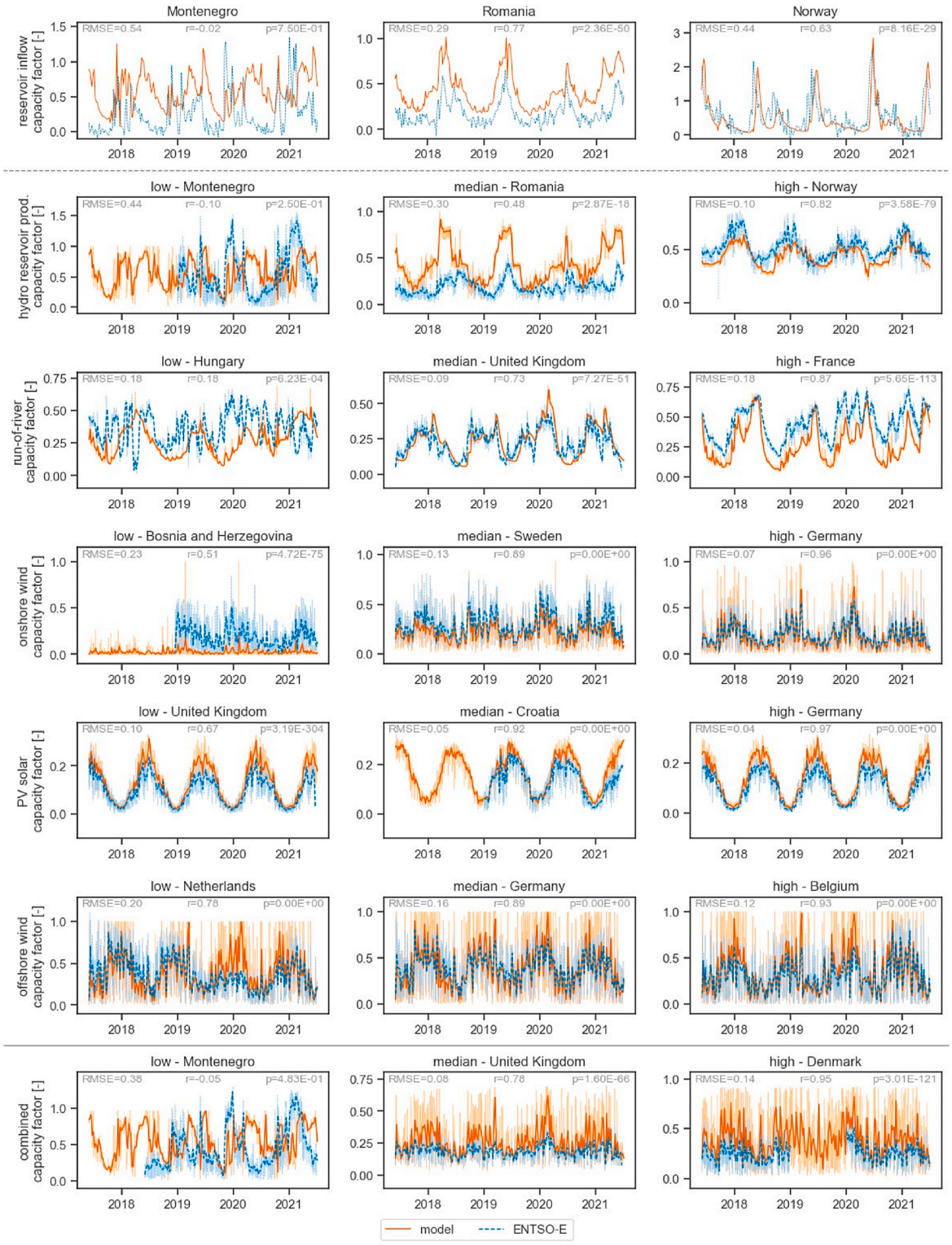

Fig. 12. Timeseries of model (orange lines) and ENTSO-E [28] derived (blue lines) renewable capacity factors for countries with relatively low (left), median (middle) and high (right) correlation values per source of energy. Plot shows a section of the timeseries from 2017 to 2022, correlation coefficient (r) p-value (p), and root mean squared error (RMSE) are computed for the full dataset from 2015 to 2022. Statistical metrics for wind, offshore wind and solar are based on daily values, and for hydropower run-of-river and reservoirs on weekly means. Thin lines represent daily values and thick lines weekly means. The reservoir inflow timeseries (top row) are added as a reference for the countries with low/median/high correlation values for hydropower reservoir production.

E event selection to the winter season (NDJFMA) (Fig. 16). In both the model and ENTSO-E winter event composite, we observe a strong pressure gradient over Northern Europe that causes low temperatures, large negative wind anomalies and moderately positive radiation anomalies. Additionally, along the southern border of France and in the North West of Spain, where many of the hydropower plants are located, we observe negative run-off anomalies [42]. analyzed the meteorological conditions driving the difference between demand and PV and wind

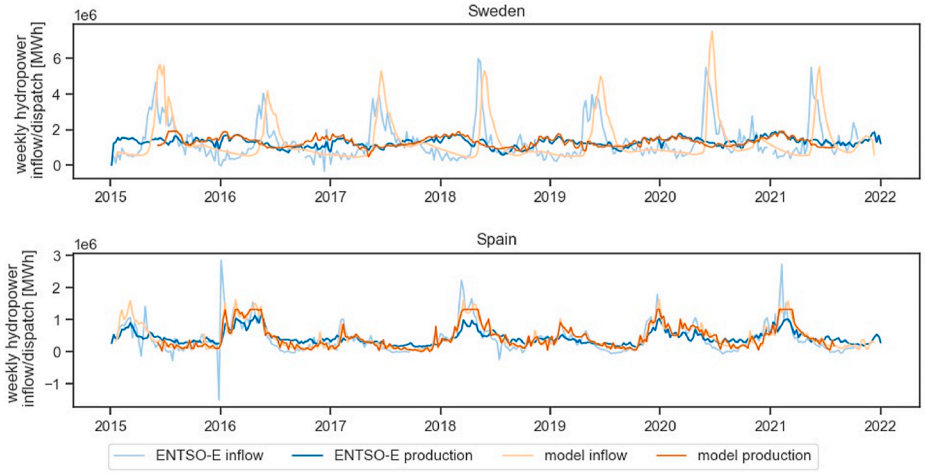

Fig. 13. Hydropower inflow and dispatch in energy units for Sweden (top) and Spain (bottom) for the years 2015–2022. With in blue the ENTSO-E derived data [28] and in orange the model results.

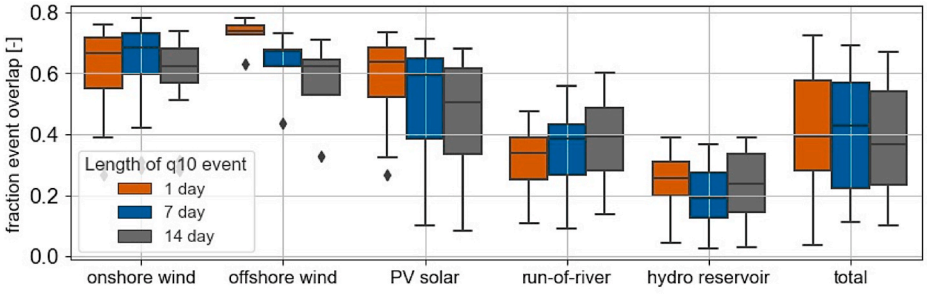

Fig. 14. Overlap between selection of events with lowest relative anomalous energy production from ENTSO-E derived data [28] and modelled electricity production.

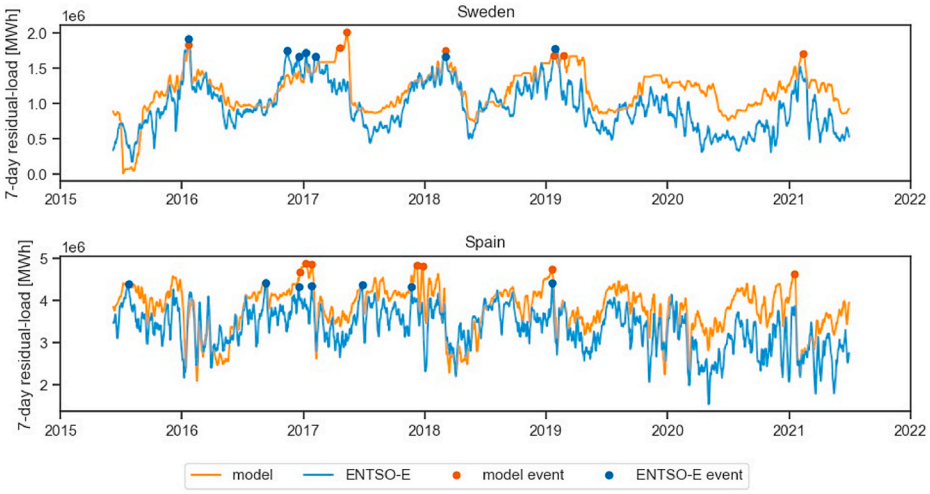

Fig. 15. Timeseries of 7-day rolling sum of difference between electricity demand and renewable production for Sweden and Spain from 2015 to 2022, with the markers presenting the top-7 (once-in-a-year) events which are a minimum of 14 days apart. Orange line/markers shows modelled time series, blue line/markers ENTSO-E data [28].

production for Spain based on ENTSO-E data, and found mostly (9 out of 10) winter events. The inclusion of hydropower generation partially shifts the extremes to summer, when short periods of meteorological drought can result in low hydropower availability due to the small storage capacities of Spain's reservoirs. For the composites of the top 7 Spanish summer events for both the ENTSO-E and model data, see Supplementary Figure E−7.

5. Limitations of the analyses

By having a strong focus on correlations over rRMSE, the evaluation procedure might have missed biases in the model. Calibrating our results

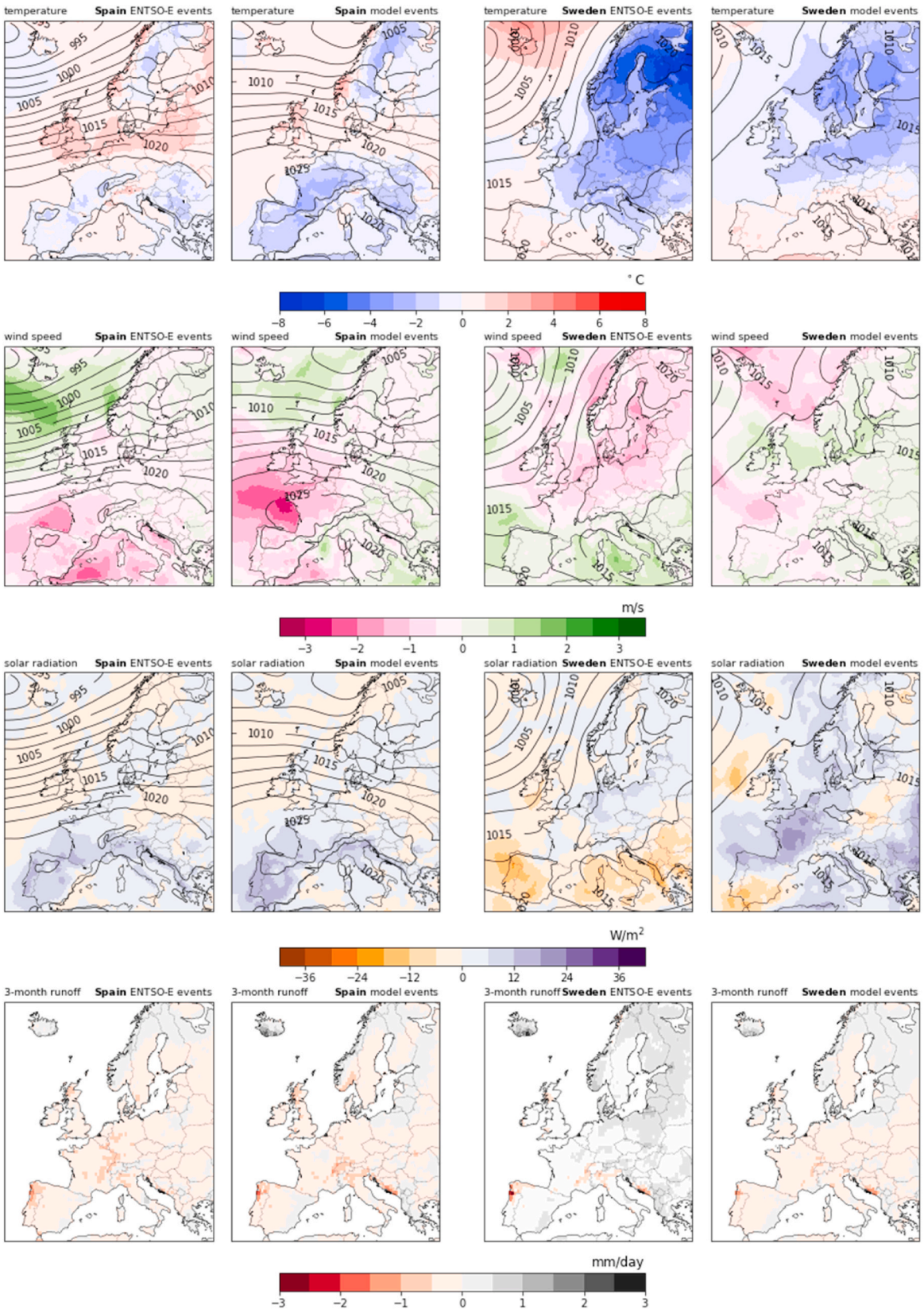

Fig. 16. *Composites of anomalies for the top 7 high residual-load winter (NDJFMA) events in Spain (left) and Sweden (right) that last 7 days, with a minimum of 14 days apart in the period of 2015-2021. Anomalies are relative to the 30-year climate (1991–2021). Composites for both ENTSO-E* [28] *and modelled events. With mean anomalies during the period of the event from top to bottom: temperature, windspeed, solar radiation, and the mean runoff in the* 3 months *before the event.*

to the ENTSO-E data would significantly reduce the rRMSEs, however, as mentioned before, the yearly installed capacities by ENTSO-E fluctuate a lot, making the validation capacity factors unreliable. We observed sudden jumps, unrealistically low-capacity factors and capacity factors above 1 (more electricity produced than the installed capacity allows for) in the ENTSO-E data.

The hydropower dispatch optimization is sensitive to installed reservoir capacities. The national hydropower reservoir capacities were determined from multiple optimization runs for which the reservoir capacity that lead to the highest correlation was selected. Especially for the countries with low correlations, this yields unreliable results. A next step could be to validate those results with literature. Additionally, the modelled dispatch is sensitive to the relative deviation difference variable that we introduce to the dispatch optimization (Fig. 5). Currently, this variable is given a randomly chosen weight of 1 for all countries, but making the weight of this variable country specific might result in more accurate dispatch patterns.

Also, we approximated flow delays by applying the same recession coefficient to all basins in Europe. Specifying this value per basin will result in better timed summer/winter peaks for reservoir and run-of-river hydropower production.

In this study we only considered the impact of meteorological variability on the production of renewable electricity. However, the efficiency of thermal power plants also has a significant dependence on variables such as air temperature, water temperature and river levels [43]. A next step could be to include the reduced efficiencies or shutdowns of these power plants due to lack of cooling water availability in the modeling framework to get better insight in the compound events that can occur.

A common problem with extreme impact events is that historical data on them is scarce. For the validation of this framework, we used the 6 available years of production and load data from the ENTSO-E platform. Consequently, validated how this framework captures the relation between meteorological conditions and energy production and demand for different regions in Europe for the past 6 years, but cannot validate its performance on more extreme (for example 1-in-20 year) events.

The intended use of the framework is scenario analysis of extreme (compound) events with large ensemble climate data, for strategic system design. To maintain reasonable computational times, sacrifices have been made in the spatial-temporal resolution. By using daily data, the implicit assumption of the framework is that there is enough storage capacity to balance the intraday variability. However, the use of daily mean values makes the framework unsuitable for the analysis of short-term extremes or to tackle operational challenges that come with meteorological variability.

Finally, the performance of the modeling framework depends on the accuracy of the input data. This validation was performed with reanalysis ERA5 and ERA5-land as meteorological input data. As reanalysis is part model-output, the data are potentially subject to biases. Using gridded observation data could improve the validation.

6. Conclusions

In this paper we have proposed and validated a new modeling framework to estimate renewable electricity production and demand from meteorological data with novel methods for the computation of hydropower production and electricity demand on days with extreme temperatures. The focus of the analyses was Europe; Spain and Sweden were highlighted in case studies.

Overall, our modeling approach characterizing reservoir hydropower operating procedures has yielded surprisingly accurate results for seasonal and interannual variability in most countries. However, for Montenegro, Bosnia and Herzegovina and Switzerland, the model does not capture the operating procedure, resulting in low model correlation with observation values. We found that the run-of-river hydropower module performs well for most (18/21) countries on modeling seasonal and interannual variability, but captures daily variability less well. The already established PV solar and wind models that we used yielded good results with correlations >0.87 for all countries.

Additionally, we performed a more detailed validation by selecting events with high residual-load for Sweden and Spain by comparing the meteorological conditions during the selected events. Although the exact dates of the modelled events and ENTSO-E events do not correspond, this case study to analyze meteorological drivers of the events yielded similar results between the two. This gives confidence in the application of the modeling framework in studies to identify driving mechanisms of (future changes in) extreme events in the European power system.

Declaration of competing interest

The authors declare that they have no known competing financial interests or personal relationships that could have appeared to influence the work reported in this paper.

Data availability

Data will be made available on request.

Acknowledgement

We would like to thank Niko Wanders for his help with the runoff routing and providing a routing scheme. This research was funded by the Energy and Sustainability Research Institute Groningen (ESRIG). This paper is written as part of the ESRIG project ICEVEPS (impact of climate extremes and variability on the European power system).

Appendix A. Supplementary data

Supplementary data to this article can be found online at https://doi.org/10.1016/j.rser.2022.112987.

References

[1] Gallo Cassarino T, Sharp E, Barrett M. The impact of social and weather drivers on the historical electricity demand in Europe. Appl Energy 2018;229:176–85. https://doi.org/10.1016/j.apenergy.2018.07.108.
[2] Orihuela R. Spanish dams at 27-year low as European energy crisis widens. Bloomberg 2022. https://www.bloomberg.com/news/articles/2022-08-23/spanish-dams-at-27-year-low-as-european-energy-crisis-widens.
[3] McGrath M. Climate change: drought highlights dangers for electricity supplies. BBC 2022, https://www.bbc.com/news/science-environment-62524551.
[4] Buli N, Jacobsen S. Analysis: weak winds worsened Europe's power crunch; utilities need better storage. Reuters; 2021. https://www.reuters.com/markets/commodities/weak-winds-worsened-europes-power-crunch-utilities-need-better-storage-2021-12-22/.
[5] Widén J, Carpman N, Castellucci V, Lingfors D, Olauson J, Remouit F, et al. Variability assessment and forecasting of renewables: a review for solar, wind, wave and tidal resources. Renew Sustain Energy Rev 2015;44:356–75. https://doi.org/10.1016/j.rser.2014.12.019.
[6] Wohland J, Eddine Omrani N, Keenlyside N, Witthaut D. Significant multidecadal variability in German wind energy generation. Wind Energy Sci 2019;4:515–26. https://doi.org/10.5194/wes-4-515-2019.
[7] Pfenninger S, Staffell I. Long-term patterns of European PV output using 30 years of validated hourly reanalysis and satellite data. Energy 2016;114:1251–65. https://doi.org/10.1016/j.energy.2016.08.060.
[8] Apadula F, Bassini A, Elli A, Scapin S. Relationships between meteorological variables and monthly electricity demand. Appl Energy 2012;98:346–56. https://doi.org/10.1016/j.apenergy.2012.03.053.
[9] Bonjean Stanton MC, Dessai S, Paavola J. A systematic review of the impacts of climate variability and change on electricity systems in Europe. Energy 2016;109:1148–59. https://doi.org/10.1016/j.energy.2016.05.015.
[10] Engeland K, Borga M, Creutin JD, François B, Ramos MH, Vidal JP. Space-time variability of climate variables and intermittent renewable electricity production - a review. Renew Sustain Energy Rev 2017;79:600–17. https://doi.org/10.1016/j.rser.2017.05.046.
[11] Emodi NV, Chaiechi T, Beg ABMRA. The impact of climate variability and change on the energy system: a systematic scoping review. Sci Total Environ 2019;676:545–63. https://doi.org/10.1016/j.scitotenv.2019.04.294.

[12] Craig MT, Wohland J, Stoop LP, Kies A, Pickering B, Bloomfield HC, et al. Overcoming the disconnect between energy system and climate modeling. Joule 2022:1405–17. https://doi.org/10.1016/j.joule.2022.05.010.
[13] Van Der Wiel K, Selten FM, Bintanja R, Blackport R, Screen JA. Ensemble climate-impact modelling: extreme impacts from moderate meteorological conditions. Environ Res Lett 2020;15. https://doi.org/10.1088/1748-9326/ab7668.
[14] Staffell I, Pfenninger S. The increasing impact of weather on electricity supply and demand. Energy 2018;145:65–78. https://doi.org/10.1016/j.energy.2017.12.051.
[15] Van Der Wiel K, Bloomfield HC, Lee RW, Stoop LP, Blackport R, Screen JA, et al. The influence of weather regimes on European renewable energy production and demand. Environ Res Lett 2019;14. https://doi.org/10.1088/1748-9326/ab38d3.
[16] van der Wiel K, Stoop LP, van Zuijlen BRH, Blackport R, van den Broek MA, Selten FM. Meteorological conditions leading to extreme low variable renewable energy production and extreme high energy shortfall. Renew Sustain Energy Rev 2019;111:261–75. https://doi.org/10.1016/j.rser.2019.04.065.
[17] Perera ATD, Nik VM, Chen D, Scartezzini JL, Hong T. Quantifying the impacts of climate change and extreme climate events on energy systems. Nat Energy 2020;5:150–9. https://doi.org/10.1038/s41560-020-0558-0.
[18] Feron S, Cordero RR, Damiani A, Jackson RB. Climate change extremes and photovoltaic power output. Nat Sustain 2021;4:270–6. https://doi.org/10.1038/s41893-020-00643-w.
[19] International Renewable Energy Agency, Union European. Renewable energy prospects for the European union. 2018.
[20] Bloomfield HC, Brayshaw DJ, Troccoli A, Goodess CM, De Felice M, Dubus L, et al. Quantifying the sensitivity of european power systems to energy scenarios and climate change projections. Renew Energy 2020;164:1062–75. https://doi.org/10.1016/j.renene.2020.09.125.
[21] Simoes SG, Amorim F, Siggini G, Sessa V, Saint-Drenan Y-M, Carvalho S, et al. Climate proofing the renewable electricity deployment in Europe - introducing climate variability in large energy systems models. Energy Strategy Rev 2021;35:100657. https://doi.org/10.1016/j.esr.2021.100657.
[22] Ho LTT, Dubus L, de Felice M, Troccoli A. Reconstruction of multidecadal country-aggregated hydro power generation in Europe based on a random forest model. Energies 2020;13. https://doi.org/10.3390/en13071786.
[23] Gøtske EK, Victoria M. Future operation of hydropower in Europe under high renewable penetration and climate change 2021:13-7.
[24] Hersbach H, Bell B, Berrisford P, Hirahara S, Horányi A, Muñoz-Sabater J, et al. The ERA5 global reanalysis. Q J R Meteorol Soc 2020;146:1999–2049. https://doi.org/10.1002/qj.3803.
[25] Teräsvirta T. Specification, estimation, and evaluation of smooth transition autoregressive models. J Am Stat Assoc 1994;89:208–18.
[26] Moral-Carcedo J, Vicéns-Otero J. Modelling the non-linear response of Spanish electricity demand to temperature variations. Energy Econ 2005;27:477–94.
[27] Silva FN, Comin CH, Costa LDF. Seeking maximum linearity of transfer functions. Rev Sci Instrum 2016;87:1–12. https://doi.org/10.1063/1.4969058.
[28] Hirth L, Mühlenpfordt J, Bulkeley M. The ENTSO-E Transparency Platform - a review of Europe's most ambitious electricity data platform. Appl Energy 2018;225:1054–67. https://doi.org/10.1016/j.apenergy.2018.04.048.
[29] Tamizhmani G, Ji L, Tang Y, Petacci L, Osterwald C. Photovoltaic module thermal/wind performance : long-term monitoring and model development for energy rating. NCPV Sol Progr Rev Meet 2003;936–9.
[30] Emeis S, Turk M. Comparison of logarithmic wind profiles and power law wind profiles and their applicability for offshore wind profiles. Wind Energy 2007;61–4. https://doi.org/10.1007/978-3-540-33866-6_11.
[31] Terink W, Lutz AF, Simons GWH, Immerzeel WW, Droogers P. SPHY v2.0: spatial processes in HYdrology. Geosci Model Dev (GMD) 2015;8:2009. https://doi.org/10.5194/gmd-8-2009-2015. 34.
[32] Oberrauch F. Hydropower design under uncertainties - communication 70. Lab Hydraul Constr 2017:175.
[33] Munoz-Sabater J, Dutra E, Agusti-Panareda A, Albergel C, Arduini G, Balsamo G, et al. ERA5-Land: a state-of-the-art global reanalysis dataset for land applications. Earth Syst Sci Data 2021;13:4349–83. https://doi.org/10.5194/essd-13-4349-2021.
[34] Dunnett S, Sorichetta A, Taylor G, Eigenbrod F. Harmonised global datasets of wind and solar farm locations and power. Sci Data 2020;7:1–12. https://doi.org/10.1038/s41597-020-0469-8.
[35] EMODnet human activities project. Emodnet_HA_WindFarms_20200305 n.d.
[36] European Commission Joint Research Centre (JRC). JRC Hydro-power database. 2019. https://doi.org/10.5281/zenodo.3862722.
[37] Danielson JJ, Gesch DB. Global multi-resolution Terrain elevation data 2010 (GMTED2010). US Geol Surv Open-File Rep; 2010. p. 26. 2011-1073 2011.
[38] Tatem AJ. WorldPop, open data for spatial demography. Sci Data 2017;4:2–5. https://doi.org/10.1038/sdata.2017.4.
[39] Leys C, Ley C, Klein O, Bernard P, Licata L. Journal of Experimental Social Psychology Detecting outliers : do not use standard deviation around the mean, use absolute deviation around the median. Exp Soc Psychol 2013;4–6.
[40] Linders MJ, Segers R, van Middelkoop M, Brummelkamp S, Keller K, Muller G, et al. Hernieuwbare energie in nederland 2020. 2021.
[41] Saint-Drenan Y-M, Wald L, Ranchin T, Dubus L, Troccoli A. An approach for the estimation of the aggregated photovoltaic power generated in several European countries from meteorological data. Adv Sci Res 2018;15:51–62. https://doi.org/10.5194/asr-15-51-2018.
[42] Bloomfield HC, Suitters CC, Drew DR. Meteorological drivers of European power system stress. J Renew Energy 2020;2020:1–12. https://doi.org/10.1155/2020/5481010.
[43] van Vliet MTH, Yearsley JR, Ludwig F, Vögele S, Lettenmaier DP, Kabat P. Vulnerability of US and European electricity supply to climate change. Nat Clim Change 2012;2:676–81. https://doi.org/10.1038/nclimate1546.